Journal of the European Ceramic Society **19** (1999) 131–137

PII: S0955-2219(98)00180-0
0955-2219/98/$—see front matter

Non-Ohmic Behaviour and Switching Phenomena in $YMnO_3$-Based Ceramic Materials

C. Moure, J. F. Fernandez, M. Villegas and P. Duran

Electroceramics Department, Instituto de Ceramica y Vidrio, (CSIC), 28500, Arganda del Rey, Madrid, Spain

(Received 31 March 1998; accepted 20 July 1998)

Abstract

Ceramic materials based on the ferroelectric compound $YMnO_3$ have been prepared by solid state reaction of the corresponding oxides to obtain sinterable powders, which were isostatically pressed and sintered at temperatures ranging from 1350 to 1525°C. The samples were characterised by X-ray diffraction, (XRD), scanning electron microscopy, (SEM), apparent density measurements, and their electrical properties were established at several temperatures. The ceramic materials showed a semiconducting behaviour when they were subject to low electrical fields. The activation energy of conductivity was calculated for a narrow range of temperatures. Applying higher electrical fields the ceramics showed non-ohmic behaviour and switching phenomena from low-to-high conductivity state with a threshold voltage which depended on the testing temperature. Values of current density as high as 80 A/cm² were measured in the high conductivity state. The process is reversible and the ceramics returned to low conductivity mode lowering or leaving the applied field. Analysis of the I–characteristic curves have allowed to advance a model based on the Poole–Frenkel effect. © *1998 Elsevier Science Limited. All rights reserved*

Keywords: ferroelectric properties, perovskites, electrical conductivity, switching phenomena, electical properties

1 Introduction

Rare earth perovskites, $LnZO_3$, (Z = Cr, Fe, Co, Mn) have been studied as potential ceramic electrodes for use in several applications, such as electrodes for magnetohydrodynamic (MHD) generation[1] and cathode material for solid oxide fuel cell (SOFC) technologies.[2–4] For this last application particular attention has been paid to the lanthanum manganite modified by Sr^{2+} or Ca^{2+} which exhibits high electrical conductivity at room temperature. Very recently great attention is being given to the giant magnetoresistance effect, which is associated to the ferromagnetic nature of some manganite perovskites.[5] However, little has been done about the effect of high electric fields on the electrical conductivity behaviour of these compounds.

The heavy rare-earth manganites (Ln = Er, Tm, Yb, Lu, and also Y), crystallise with a hexagonal structure,[6] show ferroelectric behaviour, with high T_c,[7] and are p-type semiconductors,[8] with very low conductivity values at room temperature. In a previous work the non-ohmic behaviour of the Er and Y hexagonal manganites was established on poorly densified ceramic samples.[9] A possible mechanism explaining the nature of the non-ohmic properties was pointed out. The aim of the present work is to confirm that hypothesis on well densified and ceramically characterised samples of $YMnO_3$.

2 Experimental Procedure

Submicronic powders of the Y_2O_3 and MnO oxides were used as raw materials for synthesising the manganite compounds. Stoichiometric amounts for pure $YMnO_3$ were weighted and thoroughly mixed by wet attrition milling, with isopropyl alcohol, dried and calcined at 1000°C for 2 h. The calcined cake was remilled by wet attrition. The $YMnO_3$ powder was studied by DTA and TG for establishing the O_2 evolution during the subsequent sintering of the ceramic bodies. The XRD was used for determining the crystalline structure. The size of the powder was studied by BET. Isopressed pellets were sintered from 1350 to 1525°C for several times. The shrinkage behaviour was followed by dilatometric measurement at CHR in a

Nertsz relative dilatometer model 402 E/7 from 20 to 1550°C. Apparent densities are measured by liquid displacement with water as medium. The final structure was determined by XRD. The lattice parameters were measured from the patterns. The microstructure was observed by SEM on polished and chemically etched surfaces.

From the sintered pellets thick discs were sliced, the discs were electroded with silver paste which was subsequently fired at 700°C. The *I–V* characteristic curves were established at several temperatures in an electrical furnace, by means of a shielded cell, using a DC power source (600 V, 5 A).

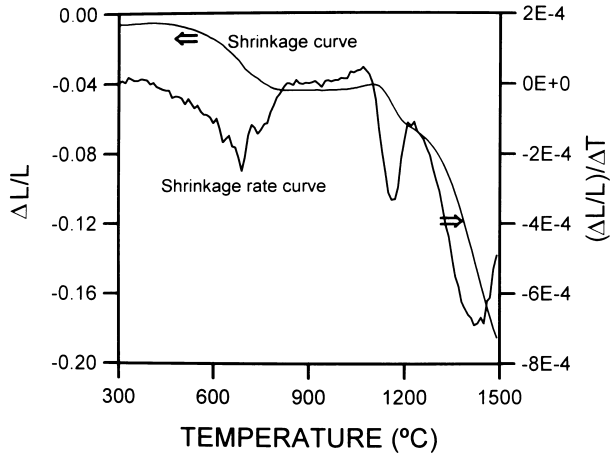

Fig. 2. Shrinkage and shrinkage rate curves taken on isopressed pellets from 20 to 1500°C.

3 Results

BET essays carried out on the attrition-milled synthesised powders gave a value of $2{\cdot}6\,m^2\,g^{-1}$, which corresponds to an average particle size of $\approx 0{\cdot}4\,\mu m$. Figure 1 shows the results of the DTA and TG essays on the synthesised powder. It can be seen the existence of an endothermic peak at 1100°C which corresponds with a weight loss which is extended until 1200°C, and is not reversible on the cooling step. This weight loss probably corresponds to the evolution of the O_2 excess respect to the stoichiometric value, 3, which was observed in the DTA analysis carried out on the oxides mixture (not shown here). Figure 2 shows the dilatometric curves corresponding to an isopressed compact. It can be seen on the shrinkage rate curve that the sintering mechanism is complex, with probably two different steps. The maximum at 700°C is probably caused by elimination of smaller pores of the green body, with a shrinkage of ≈6%. The maximum at 1200°C seems to be associated with the oxygen loss, which could cause an increment in the oxygen diffusion rate through the grain boundary. The third maximum at 1400°C, with a higher shrinkage rate can be attributed to a volume diffusion mechanism. Figure 3 depicts the densification curves as a function of temperature and time. The maximum in density is attained at 1500°C during 8 h, in a good concordance with the results of the dilatometric analysis. The attained values are relatively high, >98 D_{th}. The XRD patterns of the samples showed the existence of the hexagonal symmetry structure for all the compacts sintered at different temperatures. The XR-density was calculated from the lattice parameters measured on the XRD patterns. The calculated value was $5{\cdot}15\,g\,cm^{-3}$. Figure 4 depicts the SEM micrographs obtained on the polished surfaces. The thermally etched surfaces showed the presence of intra and intergranular cracks, whereas the chemi-

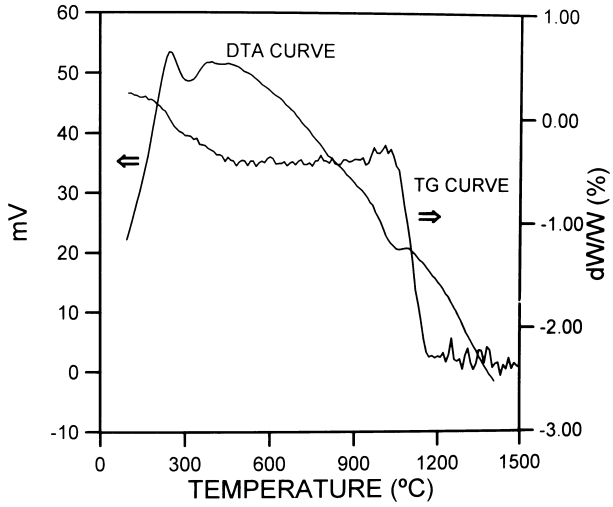

Fig. 1. DTA and TG curves obtainined on $YMnO_3$ powder previously synthesised at 1000°C.

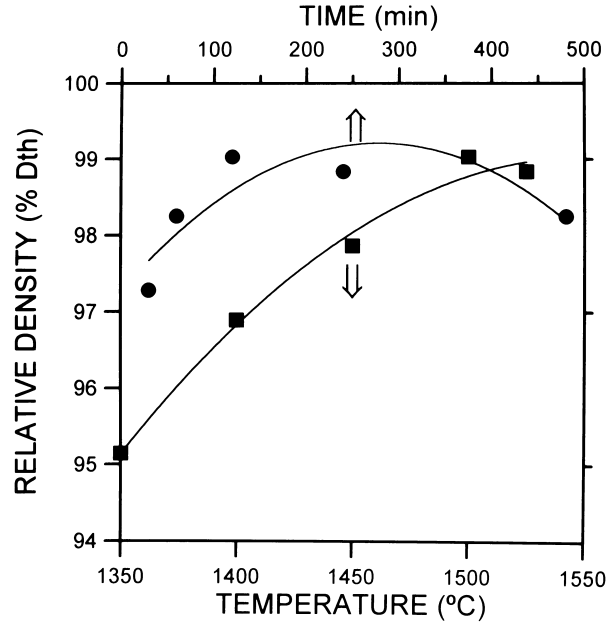

Fig. 3. Relative density curves of samples sintered at different temperatures and 2 h constant time, and at different times and 1500°C constant temperature.

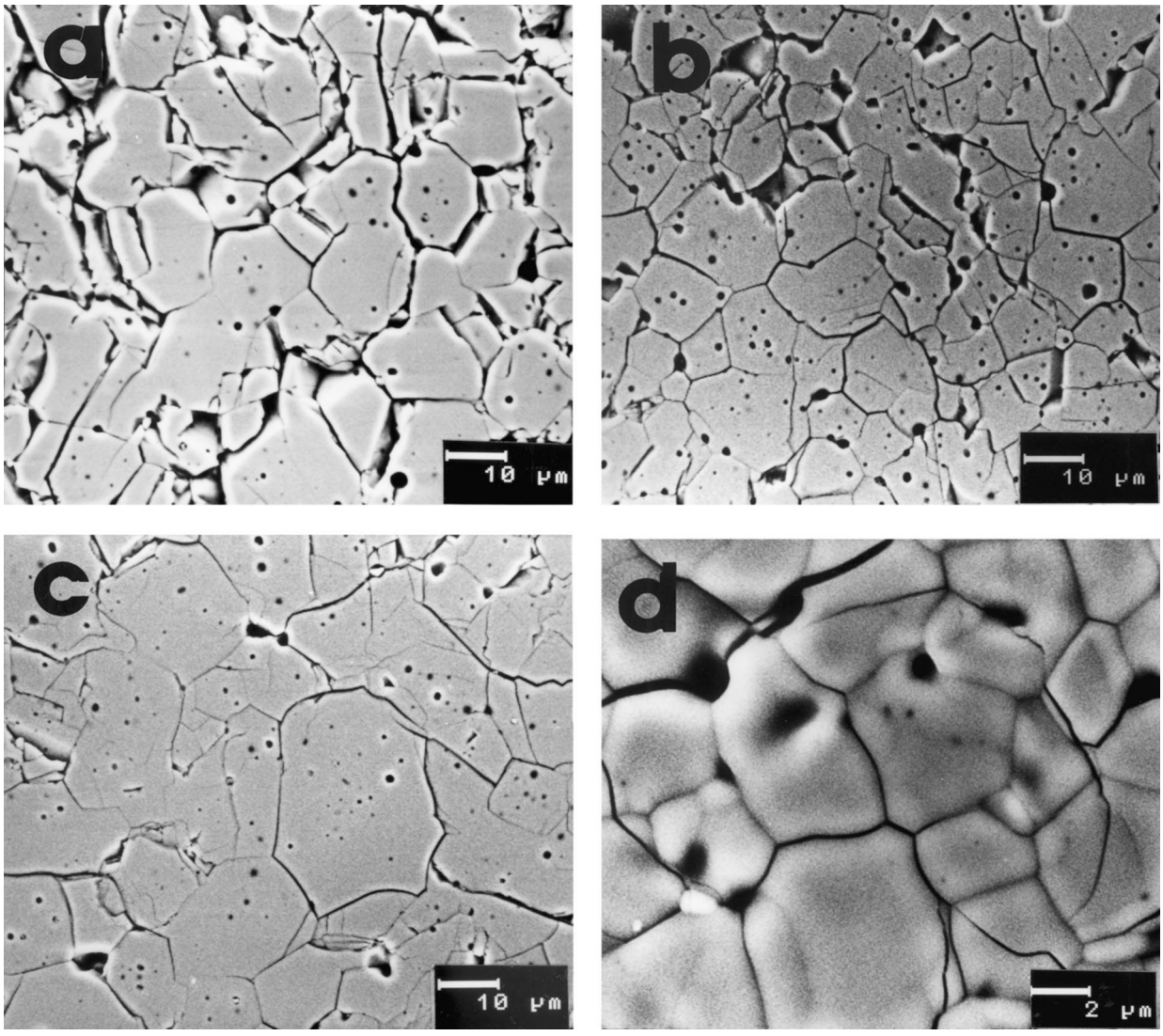

Fig. 4. SEM micrographs of (a) sample sintered at 1400°C; (b) at 1450°C; and (c) at 1500°C. The surfaces were chemically etched. (d) Sample thermally etched showing large intragranular cracks.

cally etched surfaces are free of cracks or showed only the presence of smaller cracks located preferentially in the grain boundaries. The grains have an irregular shape, and the porosity is located both in the grain boundaries and in the grain interior. The spherical shape of these pores seems to indicate that their are produced by a gas trapped in the solid, probably the oxygen released from the O_2-rich YMnO, grains. The crack appearance on the thermally etched samples, treated with cooling rates as high as $30°C\,min^{-1}$ is probably caused by the volume change (10%) which takes place during the phase transition from paraelectric phase to the ferroelectric one.[10]

Figure 5 shows the I–V characteristic curves taken on a sample sintered at 1450°C 8 h, with a apparent density value of 98% D_{th}. The measures were performed at several temperatures, from 20 to 210°C. It can be seen from the *I–V* characteristic curves that for low voltage values the sample shows a linear behaviour, which changes to a non-ohmic feature for a voltage which is decreasing when the temperature raises. Finally, it can be appreciated a region for which the current rises strongly whereas the applied voltage is keeping

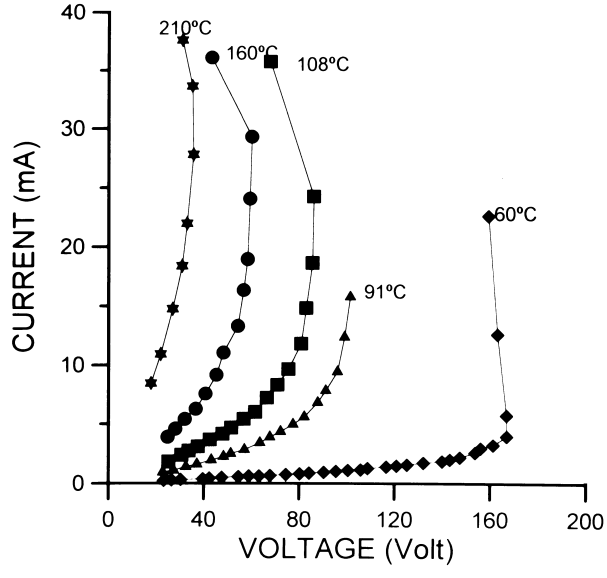

Fig. 5. *I–V* characteristic curves taken at different temperatures.

constant or lowers slightly. It was possible to determine a threshold voltage, for which the electrical conductivity switches to a high conduction state. When this high conductivity state is attained, an incandescent filamentary conduction path is clearly visible in superficial regions or inside the ceramic sample (Fig. 6). The ceramic material is strongly heated for Joule effect. Nevertheless, the filamentary path formation is a reversible phenomenon, and once that the sample is cooled and attains the initial testing temperature recover the same low conductivity behaviour such as that previous to the switching process. Therefore non permanent damage have been observed after a thermal running caused by the Joule effect. Instantaneous electrical current with values of current density as high as 80 $A\,cm^{-2}$ have been measured. Figure 7 shows the values of Ln σ and Ln σT against 1000/T. The values of conductivity were evaluated from the linear region of the I–V curves, taken at low values of V. From the Ln σT graph, activation energy value for electrical conduction was calculated to be 0·36 eV, which is lower than that reported by Rao *et al.*[8] The σ_{20} value was $3{\cdot}00\times10^{-6}$ $S\,cm^{-1}$. One has also been calculated the B coefficient, defined from the relation $\rho(T)=\rho_\infty\exp(B/T)$,[11] where ρ_∞ is the resistivity at very high temperatures. The calculated value for the $YMnO_3$ was $B=4400$ K.

As can be seen in that figure, there exist a linear relation between Ln σT and 1000/T. This relation is indicating that the $YMnO_3$ compound is a narrow band semiconductor, whose conduction mechanism is a thermally activated hopping of small polarons between localised sites, Mn^{3+}–Mn^{4+}, such as was also indicated by Rao *et al.*[8]

The curves representing Ln $(I{\cdot}V^{1/2})$ against $V^{1/2}$, corresponding to the I and V values taken on the intermediate non-linear range of the I–V curves of Fig. 5 are represented in Fig. 8. It can be seen that these curves are straight lines whose slopes have been calculated. Figure 9 depicts the slopes of the curves represented in Fig. 8 against to the inverse of the absolute temperature. It can be seen that a

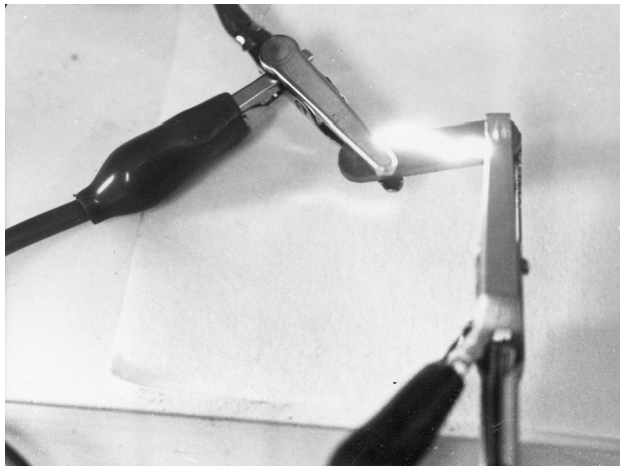

Fig. 6. Photograph taken on a sample subjected to a high electrical field, showing the filamentary conduction path.

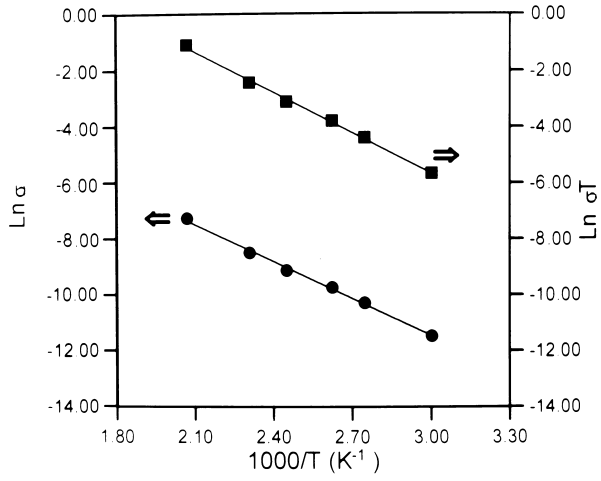

Fig. 7. Arrhenius plot of the low-field conductivity as a function of temperature.

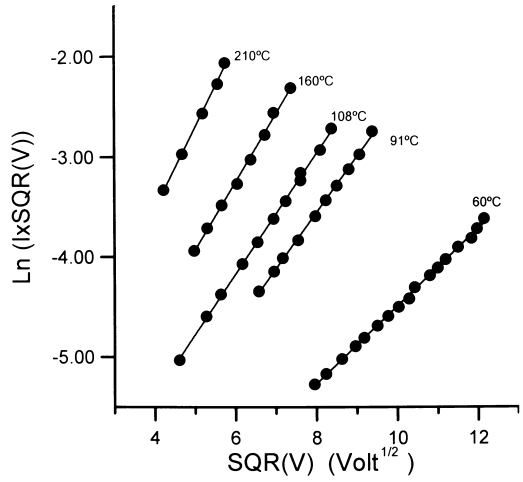

Fig. 8. $I\times V^{1/2}$ versus $V^{1/2}$ curves for values taken on the non-ohmic interval of the I–V curves shown in Fig. 5.

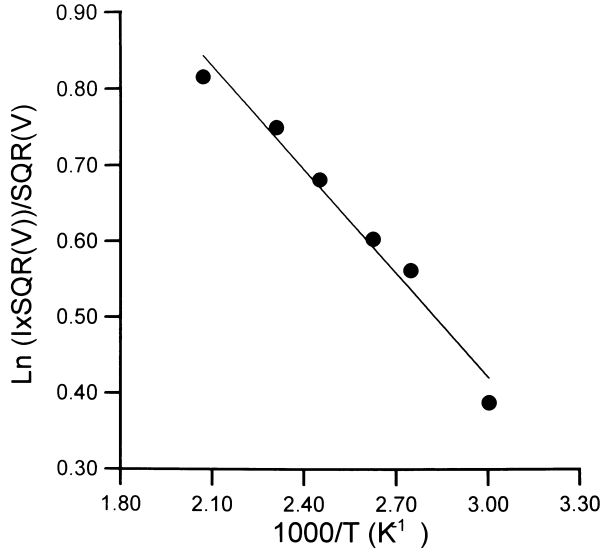

Fig. 9. $I\times V^{1\backslash2}$ $V^{1\backslash2}$ Slope versus reciprocal temperature. The slope values were calculated from the straight lines of Fig. 8.

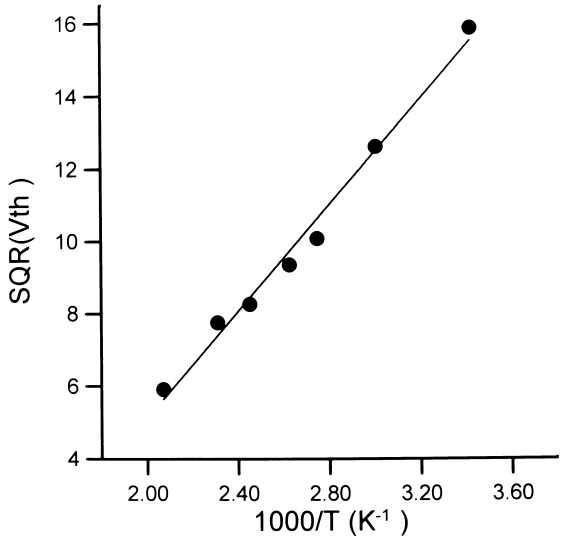

Fig. 10. Threshold voltage $(V_{th})^{1/2}$ against $1/T$.

linear relation exists, which allowed to calculate a new slope value. Finally one must mention that it have also been possible to observe a decrease of the threshold voltage when the temperature rises. Figure 10 depicts the values of $V_{th}^{1/2}$ against the inverse of the absolute temperature. The function is linear in the measured temperature interval.

4 Discussion

There are some differences been the electrical parameters, previously established by Rao *et al.* [8] and the now presented ($\rho_{200} = 8{\cdot}10^{-5}$ ohm^{-1} cm^{-1}, $E_a = 0{\cdot}63$ eV, against $\rho_{200} = 7{\cdot}10^{-4}$ ohm^{-1} cm^{-1} and $E_a = 0{\cdot}36$ eV, respectively), i.e. the electrical conductivity is higher and the activation energy is lower. Electrical parameters given for Rao *et al.*[8] were taken on polycrystalline samples sintered at 1250°C. Ceramic data were no done. During the present work it was observed very low values of apparent density for samples sintered below 1350°C. It is possible to assume that the better semiconducting behaviour here established is consequence of the higher ceramic quality.

The thermistor effect is a phenomenon appearing in semiconducting materials with NTC behaviour, (Negative Temperature Coefficient of the resistivity), which consists in the occurrence of non-linearity in the I–V characteristics, as a direct consequence of sample self heating by Joule effect. The temperature of the sample is increasing and therefore the resistivity lowers, inducing a higher value of I and further temperature raising.[11] This mechanism could be the responsible of the observed non-ohmic behaviour of the $YMnO_3$ ceramic samples.

Nevertheless, some features of this behaviour seem have not explanation only by means of the single thermistor model. The start of the non-linearity regime is at a very low current value, ($6{\cdot}5\times10^{-4}$ A at 60°C). The associated thermal energy, $P(\text{cal}) = I\text{x}V\text{x}0{\cdot}24$ is also very small ($\sim10^{-2}$ cal) and probably it cannot induce a temperature rise in the sample. On the other hand, if is taken into account the equation which correlates the maximum voltage before the start of a thermal run to the geometrical and electrical parameters of a NTC material:[12]

$$V_{\max} = A(T_0/(B - 2T_0))^{1/2} R_\infty^{1/2} \exp\{B(B - 2T_0)/2T_0(B - T_0)\} \quad (1)$$

where A is a geometrical constant, B the NTC coefficient and T_0 the equilibrium temperature, a value of 3400 V is obtained for 60°C, which is very higher than the measured value of 64 V (Fig. 5). Besides that, the non-linear region of the I–V curves can be fitted to an equation which is not supported for the thermistor model.

There is a wide literature about the switching phenomena in single oxides of transition metals from low to high conductivity state. In many cases that behaviour is associated to the existence of a metal–semiconductor transition. The switching mechanisms which govern the transition of low to high conductivity state in oxide systems are basically two:

- Release of charge carrier trapped by Schottky-type potential barrier, which are located normally in the grain boundaries of semiconducting or isolating polycrystalline solids.
- Release of charge carrier trapped on potential barrier associated to structural Frenkel-type defects, charged with an opposite sign of that ones.

In both cases the release of trapped charges is caused by the lowering of the barrier height induced by the action of an externally applied electrical field. Both mechanisms show some similitudes, and the differences are subtle. Thus, the Schottky potential barrier lowering takes place in all the possible spatial directions, as determined by the geometrical semihemisphere centred in the trapped carrier, and driving for the applied field. Therefore the probability of escape is the same for any spatial direction. This is the case of the well-known ZnO-based ceramic varistors.[13]

On the other hand, the barrier lowering on a Frenkel defect is maximum in a preferential direction of the surrounding space, whereas in the other directions the barrier height is being raised, so the escape probability of a trapped charge carrier is the maximum one in a preferred direction.

For a given electrical field E, and assuming the following conditions: the charge carrier is trapped newly for the nearest neighbour centre, it exist donors located in a deeper energy level, and finally, taking into account the non-extrinsic semiconductor nature of the $YMnO_3$ compound, the Poole–Frenkel model gives a current intensity value represented by the equation:[14]

$$I = I_o \cdot \left(C/2E^{1/2}\right) \exp\left\{(1/C) \cdot E^{1/2}\right\} \qquad (2)$$

where $C = KT/e\beta_{PF}$ and β_{PF} is the Poole–Frenkel coefficient. Figure 8 shows that there is a good linear fit on the experimental curves Ln $(I \cdot V^{1/2})$ versus $V^{1/2}$ for the values taken from the non-linear interval. On the other hand, the slope of the straight lines which can be derived of eqn (2) is $1/C = e\beta_{PF}/KT$. Such as it can be observed in Fig. 9, this relation is accomplished. As a consequence a value of the Poole–Frenkel coefficient has been calculated, giving to a $3{\cdot}84 \times 10^{-2}$ $V^{1/2}$ value. The linear relation existing between $(V_{th})^{1/2}$ and $1/T$ is indicating that there is an exponential dependence of the threshold field and the temperature. The appearance of a filamentary current path when the ceramic sample is subjected to a voltage higher than the threshold one, which is indicating that there is a certain preferred directions inside the grains for running the electrical current. That directions are communicated through the grain boundaries. Taking into account these facts, along with the recovery of the low conductivity state when the electrical field is released, without apparent damage in the ceramic body, (even after several on–off cycles), one can be assumed that the non-ohmic region could be governed by a Poole–Frenkel mechanism. The trapping centres probably are caused by the presence at different energy levels of small amounts of Mn^{2+} cations, which are located in lattice sites and associated to negatively charged oxygen vacancies. These sites could act as potential wells for the hole carrier of the $YMnO_3$ compound.

On the other hand, the very high conductivity region, far to the threshold voltage cannot be explained exclusively for that model because of the carrier concentration attains a very high value. According to Shin *et al.*,[15] the thermal running associated to the strong increase of the current density, along with the semiconductor NTC nature of the ceramic could contribute, by a feed-back mechanism to the continuous increase of the current intensity.

Nevertheless the above evidences it is necessary a lot of work for establishing more precisely the nature of mechanism governing the non-ohmic behaviour of this compound. At the present time, a series of essays on samples with different grain sizes will allow to know if there is some type of contribution corresponding to the grain-boundary-associated Schoktty barriers to the electronic conduction. Besides that, dynamic measurements with voltage pulses of different time amplitudes are being conducted for limiting the heating time caused by the increase of the current through the non-linear interval of the I–V characteristic curves.

5 Conclusions

The $YMnO_3$ compound is a narrow band semiconductor with shows a higher electrical conductivity and a lower activation energy for conduction than those previously reported. For low electrical fields shows a NTC behaviour with a high B coefficient, and a good conductivity for temperatures above the room one.

At high electrical fields it shows a non-linear behaviour which is no supported exclusively by its NTC nature. The observed switching phenomena could be explained by a Poole–Frenkel mechanism assisted by thermal running current increase in the field region far to the threshold voltage of switching.

References

1. Misuzaki, J., Sasamoto, T., Cannon, W.R. and Bowen, H. K., Electronic conductivity, Seebeck coefficient and defect structure of $LaFeO_3$. *J. Am. Ceram. Soc.*, 1982, **65**, 363–368.
2. Hammouche, A., Siebert, E. and Hammou, A., Crystallographic, thermal and electrochemical properties of the system $La_xSr_{1-x}MnO_3$ for high temperature solid electrolyte fuel cells. *Mat. Res. Bull.*, 1989, **24**, 367–380.
3. Kuo, J. H., Anderson, H. U. and Sparlin, D. M., Oxidation-reduction behaviour of undoped and Sr-doped $LaMnO_3$. Nonstoichiometry and defect structure. *J. Solid State Chem.*, 1989, **83**, 61–68.
4. Ostergard, M. J. L. and Mogensen, M., AC impedance study of the oxygen reduction mechanism on $La_xSr_{1-x}MnO_3$ in SOFC. *Electrochimica Acta*, 1993, **38**, 2015–2020.
5. Urishabara, A., Moritomo, Y., Arima, T., Asatmisu, A., Kdo, G. and Yokura, Y., Insulator–metal transition and giant magnetoresistance in $La_{1-x}Sr_{1-x}MnO_3$. *Phys. Rev. B*, 1995, **51**(II), 14 103–14 109.
6. Yakel, H. L., Koehler, W. C., Bertaut, E. F. and Forrat, E. F., *Acta Cryst.*, 1963, **16**, 957–962.
7. Coeure, Ph., Guinet, Ph., Peuzin, J. C., Buisson, G. and Bertaut, E. F., Ferroelectric properties of hexagonal orthomanganites of yttrium and rare earths. *Proc. Int. Meet. Ferroelectr*, 1966, **V**, 332–340.
8. Rao, C. N. R., Rao, G. V. S. and Wanklyn, B. M., Electrical transport in rare-earth ortho-chromites, manganites and ferrites. *Jour. Phys. Chem. Solids*, 1971, **32**, 345–358.
9. Fernandez, G., Jurado, J. R., Olmo, L. del and Moure, C., Transport electrique dans les ferroelectroceramiques $LnMnO_3$ (Ln = Er,Y). *Silicates Ind.*, 1985, **32**, 91–96.
10. Muller, O. and Roy, R., *The Major Tertiary Structural Families*. Springer–Verlag, Berlin, 1974, p. 396.
11. Moulson, A. J. and Herbert, J. M. *Electroceramics, Materials—Properties—Applications*. Chapman Tandy Hall, London, 1990, pp. 142–143.

12. Moulson, A. J. and Herbert, J. M., *Electroceramics, Materials—Properties—Applications*. Chapman Tandy Hall, London, 1990, pp. 144–145.
13. Hower, P. L. and Gupta, T. K., A barrier model for ZnO varistors. *J. Appl. Phys*., 1979, **50**, 4847–4855.
14. Coelho, R., *Physics of Dielectrics for Engineering*. Elsevier Scientific, Amsterdam, 1979, pp. 136–137.
15. Shin, S. H., Halpern, T. and Raccah, M., High speed, high current field switching of NbO_2. *J. Appl. Phys*, 1977, **48**, 3150–3153.